Environmental Science
Nano

Emerging investigator series: A multispecies analysis of the relationship between oxygen content and toxicity in graphene oxide

SCHOLARONE™
Manuscripts

Emerging investigator series: A multispecies analysis of the relationship between oxygen content and toxicity in graphene oxide

Ana C. Barrios[1,2], Yaritza P. Cahue[1,2], Yan Wang[3], Jason Geiger[3], Rodrigo C. Puerari[4], William Gerson Matias[4], Silvia Pedroso Melegari[5], Leanne M. Gilbertson[3,6], François Perreault[1,2]*

[1] School of Sustainable Engineering and the Built Environment, Arizona State University

[2] Nanosystems Engineering Research Center for Nanotechnology-Enabled Water Treatment, Arizona State University

[3] Department of Civil and Environmental Engineering, University of Pittsburgh

[4] Department of Sanitary and Environmental Engineering, Federal University of Santa Catarina, Florianópolis, Santa Catarina, Brazil.

[5] Center for Marine Studies, Federal University of Paraná, Pontal do Paraná, Paraná, Brazil.

[6] Department of Chemical and Petroleum Engineering, University of Pittsburgh

* Corresponding Author: François Perreault, francois.perreault@asu.edu

Submitted to:

Environmental Science: Nano

Abstract

The toxicity of graphene oxide (GO) has been documented for multiple species. However, GO has variable surface chemistry, and it is currently unclear whether changes in oxygen content impact GO-organism interactions the same way across species. In this study, a modified Hummer's GO (ARGO) was systematically reduced by thermal annealing at 200, 500, or 800 ℃ and toxicity towards bacteria (*Escherichia coli*), alga (*Scenedesmus obliquus*), cyanobacteria (*Microcystis aeruginosa*), and invertebrates (*Daphnia magna*) was assessed by measuring the effective concentrations inducing 50% inhibition (EC_{50}). The EC_{50}-carbon/oxygen ratio relationships show similar trends for bacteria and invertebrates, where toxicity increases as the material is reduced. Conversely, cyanobacterial inhibition decreases as GO is reduced. Further testing supports differences in cell-GO interactions between bacteria and cyanobacteria. Cyanobacteria showed a decrease in metabolic activity, evidenced by a 69% reduction in esterase activity after ARGO exposure but no oxidative stress, measured by 2',7'-dichlorodihydrofluorescein diacetate (H_2DCFDA) fluorescence and catalase activity. In contrast, ARGO induced a 55% increase in H_2DCFDA fluorescence and 342% increase in catalase activity in bacteria. These changes in cell-material interactions propose different mechanisms of action, a physical mechanism occurring in cyanobacteria, and a chemical mechanism in bacteria. The differences in GO toxicity observed in different organisms emphasize the need to differentiate the safe-by-design guidelines made for GO in relation to the potential organisms exposed.

Environmental significance:

Even though the toxicity of graphene oxide (GO) has been well documented for multiple organisms, little is known about how changes in the oxygen content alter the GO-organism interactions. This study investigates four graphene-based nanomaterials (GBNMs) of different surface chemistries and their interactions with aquatic organisms: a bacterium (*Escherichia coli*), a green alga (*Scenedesmus obliquus*), a cyanobacterium (*Microcystis aeruginosa*), and an invertebrate (*Daphnia magna*). These interactions were compared at the same biological endpoint, the EC_{50} concentration, to test whether they are the same across species. The findings emphasize how different surface chemistries and species-specific parameters alter the toxicity of GBNMs and highlight the need to consider the specific response of each organism when developing safe-by-design guidelines for GBNMs.

1. Introduction

Carbon nanomaterials (CNMs) have gained popularity due to their unique electrical, optical, and mechanical properties, leading to their widespread use in all fields of technology, from electronic systems to biomedical devices.[1–3] A class of CNMs that has been growing significantly due to the increasing number of applications is graphene-based nanomaterials (GBNMs). Their popularity is such that in 2019, the global graphene market size was estimated at 78.7 million USD and is expected to expand at a compound annual growth rate of 38.7% in the next 7 years.[4] These GBNMS include graphene, graphene oxide (GO) and their derivatives.[5,6] Graphene oxide (GO) is a highly oxidized, monolayer CNM characterized by the presence of hydroxyl, epoxy, and carboxyl functionalities along the basal plane or the edges of the graphenic structure, typically resulting in carbon to oxygen ratios (C/O) between 2-4. GO is hydrophilic and can be easily dispersed in polar solvents (i.e., water) as opposed to graphene, which has no oxygen functionalities and is hydrophobic. Reduced GO's (rGO) properties lie somewhere in between, with fewer oxygen functional groups on the carbon lattice yielding C/O ratios above 8.[3]

The wide production and application of GBNMs inevitably raised concerns regarding the potential to impart adverse consequences in the event of the unintended release to aquatic ecosystems.[7–9] The structural changes described above significantly alter the stability of GBNMs in complex environmental matrices and their interactions with microorganisms. GO has been reported to cause acute toxicity to multiple aquatic organisms including bacteria,[10–12] protozoans,[13] zooplankton,[14] adult zebrafishes,[15] zebrafish embryos,[16,17] bivalves,[18,19] algae[7,20,21], and invertebrates.[21–23] The mechanisms of interaction of GO with these different organisms have been described either as physical or chemical interactions, leading to membrane damage, cell entrapment, or oxidative stress.[24,25] However, the dominant toxicity mechanisms and material-organism interactions remain unclear and require further investigation.

Previous studies have shown that surface chemistry and presence or absence of functional moieties in CNMs play an important role in establishing their biological activities.[8,26–30] Gilbertson et al. for example, demonstrated the ability to control the biological activities of oxygen functionalized multi-walled carbon nanotubes (O-MWCNTs), another type of CNMs, by controlling their surface chemistry with either strong acids or high temperature annealing.[28,31] In a similar study, Wang et al. performed a systematic reduction of GO materials through thermal annealing to vary the C/O ratio from 1.58 to 5.80 to further understand the relationships that correlate the materials' properties to both their performance and inherent hazards.[8]

Given the wide diversity in GBNMs' structure, morphology, and composition, it is of utmost importance to understand the structure-activity relationships that underline the potential toxicity of nanomaterials (NMs). Unraveling how changes in the structural or morphological properties of GBNMs can affect their interactions with living cells will help us estimate the biological hazard and subsequent risk of new NMs. With this in mind, we recently investigated the structure-property-toxicity relationships for a suite of GO materials, systematically reduced using thermal annealing, in a bacterial model, *Escherichia coli* (*E. coli*). This previous study demonstrated higher bacterial toxicity as GO is reduced, with lower effective concentration inducing 50% decrease in bacteria viability (EC_{50}) as the C/O ratio increased.[27] This structure-property-toxicity relationship, however, was only demonstrated in bacteria, which is one type of microorganism present in aquatic environments. Whether the same responses can be translated to other aquatic organisms or not is still unknown.

In this study, we compare how the differences in oxygen content of a modified Hummer's GO (ARGO) and three thermally annealed GOs (TGO200, 500, and 800) alter the toxicity towards multiple aquatic species including a bacterium, a green alga, a cyanobacterium, and an invertebrate. The selected model organisms are *E. coli, Scenedesmus obliquus (S. obliquus), Microcystis aeruginosa (M. aeruginosa)* and *Daphnia magna (D. magna)*, which are all organisms that are commonly used for aquatic risk assessment thanks to their sensitivity, ecological relevance, and short generation spans.[32] With this suite of biological assays, we show that the structure-property-toxicity relationships established in one model may not always be applicable to other organisms due to the differences in the model-specific mechanisms of interactions involved.

2. Materials and methods

2.1 Chemicals. All the fluorescent dyes were obtained from Thermo Fisher Scientific (Molecular Probes, Eugene, OR). The dyes include fluorescein diacetate (FDA), and 2',7'-dichlorodihydrofluorescein diacetate (H_2DCFDA). Unless specified, all chemicals were dissolved in deionized (DI) water obtained from a GenPure UV xCAD plus ultrapure water purification system (Thermo Scientific, Waltham, MA). A modified Hummer's powdered single layer GO (~99% pure) was purchased from ACS Materials LLC (Medford, MA, USA, product no. GNOP10A5) and used as received (ARGO). Surface modification on the GO was prepared by thermally treating the ARGO under helium (He) gas flow in a tube furnace (Thermo Scientific Lindberg/Blue M TF55035A-1) with a custom-built quartz tube at increasing temperatures 200, 500, and 800 °C.[8] The ARGO was added to the quartz tube and heated at a rate of 5 °C min^{-1} to the maximum temperature, held for 30 min, and left to cool at room temperature under He flow. These thermally reduced GO samples are referred to as TGO200, TGO500, and TG800, respectively.

2.2 Material characterization. X-ray Photoelectron Spectroscopy (XPS) was done for all the GBNMs to identify changes in the materials' surface chemistry. XPS offers a quantitative approach to evaluate the reduction degree of ARGO as a function of thermal annealing. Further, multiple batches of each material were prepared for carrying out the toxicity assays, making sure to use the same batch for each taxon studied. For XPS analysis, the sample holder was covered with double-sided copper tape and dusted with enough GO powdered material to cover the surface. The sample was then loaded in a Thermo Scientific ESCALAB 250Xi that uses a monochromatic Al Kα X-ray source with the following parameters: 1486.7 eV and a spot size of 650 μm. Survey spectra were collected using a 1.0 eV step size and 150 eV pass energy while a 0.1 eV step size and 50 eV pass energy were used for the high resolution spectra. Three measurements in different locations were collected per sample. The Thermo Scientific Avantage software was used for peak fitting and to calculate the atomic percentage.[8] The GBNMs were characterized using Scanning Electron Microscopy (SEM) to determine the size of the GO sheets. The SEM images were taken with an Amray 1910 FE-SEM using 10 eV. For sample preparation, 3 μL of a diluted 50 μg/mL GO stock solution was drop-casted on a 1 cm × 1 cm silicon wafer previously cleaned via UV-ozone treatment for 20 min (UV/Ozone ProCleaner, BioForce Nanosciences, Ames, IA). The ImageJ software was used to process the SEM images and measure GO dimensions.

2.3 Toxicity of GBMNs to *E. coli*. The antimicrobial suspension assays were done according to Barrios et al.[27] *E. coli* W3110 (American Type Culture Collection ATCC 11303) was grown overnight in Lysogeny Broth (LB) on a shaker plate at 140 rpm in an Isotemp incubator (Fisher Scientific) at 37 °C. Then, the culture was diluted in fresh LB (1:25) and grown until the optical density (OD) reached 1 (~2 h). Cells were washed with sterile 0.9% NaCl solution three times by centrifugation. The bacterial solution was then diluted to 10^7 colony-forming units (CFUs)/mL in sterile saline solution.

For GO exposure to the bacteria, stock suspensions of ARGO and each TGO materials were made in nanopure water (5,000 μg/mL) and bath sonicated for 1 h (M3800 Branson Ultrasonic Corporation, Danbury, CT). The exposure took place in a total volume of 5 mL, where 3.5 mL of sterile 0.9% NaCl, 0.5 mL of clean bacteria solution, and then supplemented with the required volume of each GO suspension to reach concentrations of 1, 10, 50, 150, 250, and 500 μg/mL in 7 mL scintillation vials. A negative control (no GO added) treatment was created by adding 1 mL of sterile DI water. Vials were placed on a horizontal shaker (Branstead Lab-Line) at 80 rpm for 3 h and kept at room temperature. After the 3 h contact time, the bacteria-GO suspensions were diluted (1:10) in Eppendorf tubes and vortexed, and 50 μL of each suspension was spread on a LB agar plate and incubated overnight at 37 °C for CFU enumeration.

2.4 Toxicity of GBNMs to aquatic photosynthetic microorganisms. The freshwater cyanobacteria *M. aeruginosa* (UTEX LB 3037) and green alga *S. obliquus* (UTEX 3031) were both grown and maintained in sterile Bold Basal Medium (BBM) with a pH of 6.8, at a controlled temperature of 28 ± 2 °C, and a constant illumination of 4.85 ± 0.31 mW/cm^2 (Thorlabs, NJ, USA), as previously described.[33] Constant aeration was provided by air bubbling, filtered by a 0.20 μm sterile cellulose filter (VWR, USA), using an aquarium pump (Whisper Air Pump, Tetra, USA). The cultures were diluted once a week with fresh BBM medium to maintain a constant algal growth in the stock solution. To assess the

cultures' growth, the relationship between cell density and optical density at 750 nm was measured. Cell density was measured by adding 5 µL of each culture in a hemocytometer and counting the cells with a Leica DM6 epifluorescence microscope (Leica Microsystems, Inc. Buffalo Grove, IL) in bright field mode.

For GO exposure, the algal cultures were diluted to 5×10^5 cells/mL and allowed to grow until the mid-exponential phase (~ 2h, monitored by optical density at 750 nm). Stock suspensions of ARGO and each TGO materials were made in nanopure water (2,000 µg/mL) and bath sonicated for 72 h (M3800 Branson Ultrasonic Corporation, Danbury, CT). In 50 mL Erlenmeyer flasks, 18 mL dilution of 2×10^6 cells/mL is made from the stock solution of *M. aeruginosa* and BBM medium. Then, a volume of the stock GO suspension was added to reach concentrations from 1, 5, 10, 25, 50, and 100 µg/mL in a total volume of 20 mL, supplementing with sterile BBM to 20 mL, as needed. A control (no GO added) treatment was made by adding 2 mL of sterile BBM into the 18 mL algal dilution. Flasks were kept at a constant temperature (28 ± 2 °C) on a shaker at a speed of 60 rpm for 96 h. After the 96-h contact time, 1.5 mL of the algae-GO aliquots were collected in 2 mL Eppendorf tubes, centrifuged for 10 min, and the supernatant was removed, keeping the algal cells and the GO in the pellet. Then, 0.5 mL of methanol were added to the Eppendorf tubes, vortexed, placed on a digital dry bath (Fisher Scientific Waltham, MA) set at 70°C for 10 min, and centrifuged again for 10 min to pellet the cell debris. A 0.2 mL volume of the pigment extract (supernatant) was placed in a transparent microplate to measure chlorophyll *a*, chlorophyll *b*, and total chlorophyll concentrations on a microplate reader (Synergy H4, BioTek) according to Lichtenthaler.[34]

2.5 Toxicity of GBNMs to *D. magna*. The freshwater microcrustacean *D. magna* was maintained according to ISO 6341[35] and NBR 12.713.[36] All animal procedures were performed in accordance with the Guidelines for Care and Use of Laboratory Animals at the Federal University of Santa Catarina. For studies with *D magna*, according to the university guidelines, evaluation by the ethics committee is not required. The organisms were kept in M4 medium at controlled temperature (20 ± 2 °C) and diffuse luminosity with a photoperiod of 16h of light and 8h of darkness. The *D. magna* was fed three times a week with approximately 10^6 cells/mL per organism using *Scenedesmus subspicatus* algal culture.

Prior to the acute toxicity tests with *D. magna*, ARGO and each TGO samples were diluted in ISO medium, according to NBR 12.713.[36] The stock suspensions (500 mg/L) were bath sonicated (Ultrasound bath, model Q3360, QUIMIS, São Paulo, Brazil) at 70 W for 4h. In the assays, offspring of *D. magna* (2-26h old) were exposed to concentrations of 12.5, 25, 50, 100, 200, and 400 mg/L. The negative control was conducted with ISO medium only (no GO added). For each dilution, 20 *D. magna* offspring were exposed (duplicates of ten organisms) for a period of 48 h. The toxicological endpoint was the immobilization of the organisms. The data were statistically analyzed using the Trimmed Spearman-Karber method and the results were expressed as $EC_{50,48h} \pm$ Standard Deviation. The acute toxicity tests were conducted three times for each material. The sensitivity of the organisms was assessed using potassium dichromate ($K_2Cr_2O_7$) as reference substance and with exposure for 24 h. For the organisms used in this research, the result was $EC_{50,24h} = 0.94 \pm 0.17$ mg/L, within the recommended range for validating the results (0.6 mg/L to 1.7 mg/L).

2.6 Experimental conditions. A literature review was performed to compile the different experimental conditions commonly used for studying the toxicity of GO and its material derivatives (i.e., reduced GO, graphene) for each organism (*E. coli*, *M. aeruginosa*, *S. obliquus*, or *D. magna*), including parameters and endpoints employed (Table S1). Three main observations emerged: 1) Experimental conditions (time and manner of exposure, and materials' concentrations) vary across organisms; 2) The extent of material characterization is not uniform; and 3) There are many toxicity endpoints used to measure the response of an organism towards a material. This data collection informed our selection of conditions for this study facilitating comparison to the existing literature (Table 1). The four organisms were selected to represent their respective taxa. Bacteria, algae, and aquatic invertebrates are attractive for toxicity characterization because their generation spans are shorter than those of higher organisms like fish.[32] Additionally, toxicity tests using these

organisms usually require smaller volumes and thus, require smaller quantities of NMs. The range of GBNMs' concentrations we investigated showcases the different sensitivities of each organism towards GO.

The literature survey also highlighted the gaps in materials characterization reporting in GBNMs' toxicity studies. While it is common practice to report characterization parameters like GBNMs' thickness, lateral size, and defect density (i.e., D/G ratio), the focus on surface chemistry is less frequently found. The carbon-to-oxygen ratio or C/O ratio has been identified as a key parameter to better understand the relationship between surface chemistry and toxicity for GBNMs[27] but it is not comprehensively studied. Thorough material characterization is necessary to identify further indicators that will help in safer material design. Therefore, this study utilizes the same material set, ARGO and thermally annealed ARGOs, which are compared across all the chosen organisms that represent different taxa. The systematic reduction of ARGO produces GBNMs of different surface chemistries.

Table 1. Experimental conditions for each organism tested.

Organism	Taxon	Medium	Contact time (h)	Concentrations (µg/mL)	Parameter used for EC_{50}
E. coli	Bacteria	0.9 % NaCl	3	0-500	CFU enumeration
M. aeruginosa	Cyanobacteria	BBM	96	0-100	Chlorophyll
S. obliquus	Algae	BBM	96	0-100	Chlorophyll
D. magna	Invertebrate	ISO	48	0-400	Immobilization

2.7 Aggregation experiments. Aggregation experiments were performed with ARGO in the respective media used for toxicity assays: 0.9% NaCl (bacteria), BBM (algae/cyanobacteria), and ISO medium (invertebrate). No organisms were included, and experiments were performed at ambient temperature. ARGO stock solutions (2000 µg/mL in DI water) were bath sonicated for 1 h (150HT Ultrasonic Cleaner, Aquasonic, USA). An experimental concentration of 100 µg/mL was used in all media. Additional concentrations of 200 µg/mL for 0.9% NaCl, 10 and 40 µg/mL for BBM (for *M. aeruginosa* and *S. obliquus* respectively), and 400 µg/mL for ISO medium were studied, representing the respective EC_{50} values. Hydrodynamic diameter (D_h) was analyzed 5 min after the addition of ARGO stock and at the end of the respective toxicity assay duration: 3 h for bacteria, 96 h for algae, and 48 h for daphnia. All experimental samples were agitated according to details specified in toxicity assays. Experiments were performed in triplicates with 5 mL solution in 7 mL scintillation vials for ISO medium and 0.9% NaCl, and 20 mL solution in 50 mL Erlenmeyer flasks for BBM. The respective volumes were selected based upon the experimental setups of the toxicity assays. In the interest of conserving materials, the volume of ISO medium differed based on the lack of motion limiting the potential for variability. The ARGO aggregate size was measured using dynamic light scattering (DLS, Litesizer 500, Anton-Paar, Austria) to obtain D_h. All measurements were determined at a 90° detection angle. Spectra were averaged over 12 scans. UV-vis analysis of sample solutions was performed, showing negligible absorption at the LiteSizer 500 light wavelength (658 nm). Fourier transform infrared (FTIR) spectroscopy (Bruker IFS66 V/S, USA) equipped with an MCT detector and a KBr beam splitter with a Diamond Attenuated Total Reflectance (ATR) module was done to assess changes in the materials' surface chemistry after being added to each media.

2.8 Effective concentration calculation. The software OriginPro 8.5.1 was used to calculate the EC_{50} in bacteria and alga/cyanobacteria experiments. Data fitting was done using a sigmoidal fit using the dose-response function with the following equation:[37]

$$y = A1 + \frac{A2 - A1}{1 + 10^{(log_x0 - x)p}} \tag{1}$$

Where A1 = bottom asymptote, A2 = top asymptote, log_x0 = center, p = hill slope, and EC_{50} is given by:

$$EC_{50} = 10^{log_x 0} \tag{2}$$

For invertebrates, the EC_{50} values were calculated through the Trimmed Spearman-Karber method, after Hamilton et al.[38]

2.9 Fluorescent dye assays after GBNMs exposure. To further investigate biochemical responses of bacteria and cyanobacteria to GO, a set of fluorescent dyes were used at the EC_{50} concentrations of either *E. coli* or *M. aeruginosa* after exposure to ARGO and TGO800 (bacteria) or TGO500 (cyanobacteria). Changes in esterase activity and membrane damage and oxidative stress were evaluated using the FDA and H_2DCFDA fluorescent dyes, respectively.[39] Stocks solutions for each dye were prepared according to the manufacturer specifications (Molecular Probes™, Thermo Fisher, Waltham, MA): 10 mM for FDA and H_2DCFDA and kept at -20°C in the dark. After the exposure time (3h for bacteria, 96h for cyanobacteria), 1 mL of the cells were stained with a final concentration of 5 mM of FDA or 0.2 mM H_2DCFDA. The samples were incubated for 30 min in the dark before pipetting 200 μL of each sample in a 96 well plate. The fluorescence was measured using excitation/emission wavelengths of 490/526 nm for FDA and 495/527 for H_2DCFDA on a multi-mode microplate reader (Synergy H1, BioTek). Data was expressed as the mean fluorescence intensity and the results as a percentage with respect to the control.

2.10 Catalase activity after GBNMs exposure. CAT activities were measured for *E. coli* and *M. aeruginosa* after exposure to ARGO and TGO800 (bacteria) or TGO500 (cyanobacteria) at their EC_{50} concentrations. For the antioxidant enzyme measurements, 2 mL of either bacterial or cyanobacterial cell suspensions were collected in Eppendorf tubes after the allocated contact time (3h or 96h). Samples were centrifuged (5,000×g, 1 min) to form a pellet and then washed three times with 1 mL of 50 mM phosphate buffer (pH = 7.4). Cells were homogenized using bath sonication (M3800 Branson Ultrasonic Corporation, Danbury, CT) for 30 min kept at 4 °C using ice and then centrifuged at 5,000×g at 4 °C for 1 min. The supernatant was used for biochemical analysis. CAT activity was evaluated spectrophotometrically by the decomposition rate of hydrogen peroxide (H_2O_2) at 240 nm at 25 °C according to Aebi.[40] Total soluble protein was measured using the Pierce™ BCA Protein Assay Kit (Thermo Scientific No. 23225).

2.11 Electron microscopy of cells after GBNMs exposure. The effect of GO exposure on cell morphology was evaluated for *E. coli* and *M. aeruginosa* after contact to ARGO and TGO800 (bacteria) or TGO500 (cyanobacteria) using SEM and TEM imaging. Cultures were prepared depending on the parameters used for the toxicity assays using the 3h and 96h EC_{50} concentrations. At the end of the contact time, cells were collected by centrifugation (5,000×g, 1 min) and the pellet fixed in Karnovsky's fixative (2% paraformaldehyde, 2.5% glutaraldehyde in 0.2 M Sorenson's buffer, pH= 7.2) overnight at 4°C.

For SEM imaging, the fixed cells were washed once with Dulbecco's Phosphate Buffered Saline (DPBS), adhered to poly-L-lysine coated coverslips, and then washed two additional times with DPBS. Secondary fixation was done with 1% OsO_4 in DPBS for 1h at room temperature, followed by three washes with DI water. Cells were dehydrated with an ascending series of ethanol solutions followed by critical-point drying using a CPD-020 unit (Balzers-Union, Principality of Liechtenstein) with liquid CO_2 as the transition fluid. The dried samples were mounted on aluminum stubs and coated with 10-12 nm of gold-palladium using a Hummer II sputter coater (Technics, San Jose, CA). Imaging was done on a JSM 6300 SEM (JEOL USA, Peabody, MA) operated at 15 kV and images were captured with an IXRF Systems model 500 digital processor (IXRF System Inc., Austin, TX).

For TEM imaging, the fixed cells were pelleted and entrapped in 0.8% agarose before washing three times with DPBS. Cell pellets were then fixed with 1% OsO_4 in DPBS for 2h at room temperature and rinsed four times with deionized water. The cells were stained overnight at 4°C using 1% aqueous uranyl acetate and washed the following morning with 4 changes of DI water. Cells were dehydrated with an ascending series of ethanol concentrations (20, 40, 60, 80, 100% ethanol), rinsing three times with 100% ethanol. Then, the 100% ethanol was replaced twice with propylene oxide before infiltrating the samples in increasing concentrations of Spurr's standard mixture epoxy resin[41] using 25% increments. Embedded samples were polymerized at 60°C for 24 hrs. Resin blocks were microtomed to 70 nm sections with a Leica Ultracut-R microtome (Leica

Microsystems, Buffalo Grove, IL) and collected on formvar-coated copper slot grids. Microtomed sections were stained with 2% uranyl acetate in 50% ethanol for 6 min followed by Sato's lead citrate[42] for 3-4 min. Images were obtained using a Philips CM12 TEM (Philips, Eindhoven, Netherlands) operated at 80kV. Micrographs were acquired with a Gatan model 791 CCD camera.

2.12 Data analysis and statistics. All experiments were done using triplicate samples and in three independent experiments at a minimum. Data is shown as means and standard deviation, calculated for each treatment. A one-way analysis of variance (ANOVA) followed by a Tukey post-hoc test with $p<0.05$ was done to determine significant differences between control samples and GO treated samples. These differences were indicated using different letters in the figures. Statistical analysis was done using the Statistical Package for Social Sciences (SPSS) software version 26.

3. Results and discussion

3.1 Surface chemistry characterization of GBNMs. The different GBNMs were characterized by XPS to identify how the surface chemistry of ARGO and TGOs influence their interaction with different organisms. XPS offers a quantitative approach to evaluate the reduction degree of ARGO as a function of thermal annealing. Further, multiple batches of each material were prepared for carrying out the toxicity assays, making sure to use the same batch for each taxon studied. Surface characterization is important to ensure that the desired trend in O% is attained (Table 2 for C/O ratio and Table S2 for full chemical composition). The C% in all annealed materials increased significantly as the annealing temperatures increased. The C% were in the ranges of 66-71% for ARGO, 80-82% for TGO200, 85-88% for TGO500, and 83-92% for TGO800. These results were accompanied by a decrease in O% with ranges of 28-33% for ARGO, 17-18% for TGO200, 12-13% for TGO500, and 7.5-12% for TGO800.

The C/O ratio (Table 2) serves as an indicator of the degree of surface reduction. Different batches of material sets were used per organism (same batch for both photosynthetic organisms). Results show that no significant differences were found across batches for ARGO, TGO200, and TGO500. TGO800 had a significant increase in C/O ratio between the batch used for bacteria (7.19 ± 0.11) and the batches used for algae and invertebrates (11.7 ± 1.68, 12.0 ± 1.00), respectively. Even with these differences, all material batches follow the same trend where the increase in C/O ratio from ARGO<TGO200<TGO500<TGO800 confirms successful deoxygenation of the ARGO surface and indicates restoration of the conjugated carbon structure.[43] These results are in accordance with previous studies, where thermal annealing systematically reduces the O% of ARGO as the temperature increases.[8,27] Furthermore, peak deconvolution of the C1s spectra determined the relative presence of different carbon-oxygen bonds for all GBNMs (Table S2). The deconvolution of C1s resulted in four peaks located approximately at binding energies of 284.8, 286.3, 287.5, and 288.8 eV which are commonly assigned to single and double carbon bonds (C-C/C-H), epoxide and hydroxyl (C-O), carbonyl (C=O), and carboxylate (COOH) functional groups, respectively.[8,27] The content of C-O groups, including epoxide and hydroxyl groups on the GO basal plane, decreases consistently across batches from 41.89% for ARGO to 8.18% for TGO800 upon thermal annealing. This decrease can be attributed to the reduction of epoxide groups, which are the most abundant on GO surfaces[8,44] and are not chemically or thermally stable.[8] At the highest temperature used (800°C), C-O bonding contributes the highest fraction (in a range from 8.18 to 9.75%) compared to C=O (from 3.53 to 4.58%) and COOH (from 1.49 to 1.62%) across batches. This has been observed in previous studies and is attributed to the higher thermal stability of hydroxyl groups intercalated into graphene interlayers.[8,44] The carbonyl and carboxylate groups, mostly found in the edges of the GO structure, exhibit a steady decrease upon thermal reduction.

Elemental survey by XPS also revealed the presence of other residual elements on the materials' surface: sulfur (S%), nitrogen (N%), and sodium (Na%) (Table S3). These impurities are most likely from the precursors used during the synthesis of the GO. A commercial GO material synthesized by a modified Hummers method was used, and typical reagents used for the modified Hummers reaction include H_2SO_4, $NaNO_3$, and $KMnO_4$.[43] All ARGO materials were of 98.5% purity or higher before thermal annealing. Thermal annealing of ARGO at any of the temperatures used (200, 500, or 800 ºC) had no significant effect on the materials' sheet size and the average lateral sheet was of 1.2 ± 0.7

µm for the most oxidized material (ARGO) and 1.1 ± 0.7 µm for the most reduced material (TGO800).[27]

Table 2. Compiled XPS data representing the C/O atomic ratio for ARGO and TGO samples. Data is shown as means ± standard deviations of triplicate measurements. Different letters indicate statistical difference at p ≤ 0.05 between the same material across batches.

	Bacteria	Algae/Cyanobacteria	Invertebrates
ARGO	2.02 ± 0.06 [a]	2.01 ± 0.07 [a]	2.54 ± 0.59 [a]
TGO200	4.41 ± 0.31 [a]	4.64 ± 0.09 [a]	4.70 ± 0.13 [a]
TGO500	6.48 ± 0.62 [a]	7.61 ± 0.24 [a]	7.48 ± 0.59 [a]
TGO800	7.19 ± 0.11 [a]	11.7 ± 1.68 [b]	12.0 ± 1.00 [b]

3.2 Toxicity of GBNMs differs across species. The toxicity of the GBNMs to *E. coli*, *M. aeruginosa*, *S. obliquus*, or *D. magna* was characterized according to the parameters shown in Table 1. For all species, the EC_{50} was selected as the biological endpoint to compare toxicity. For bacteria, the antimicrobial properties of ARGO and TGOs were assessed by mixing *E. coli* with GBNMs suspensions of concentrations ranging from 0 to 500 µg/mL for 3h to generate a dose-response curve. A sigmoidal fit was used to calculate the EC_{50} value per material. The EC_{50} was characterized by a reduction of bacterial cell viability determined by a decrease in colony forming units (CFU). Figure 1 shows that each material reduced bacterial viability by 50% at different concentrations (red squares). According to the dose-response curves, the calculated EC_{50} values were 183 ± 33.9 for ARGO, 143 ± 24.8 for TGO200, 127 ± 11.0 for TGO500, and 86.3 ± 28.9 µg/mL for TGO800.

D. magna, a model organism for aquatic invertebrates, was exposed for 48h to GBNMs suspensions with concentrations from 0 to 400 µg/mL. The calculated EC_{50} values were 383 ± 29.9 for ARGO, 187 ± 18.3 for TGO200, 319.8 ± 14.4 for TGO500, and 263.2 17.0 µg/mL for TGO800 (blue triangles). It is worth noting that the TGO200 value for *D. magna* was found to be an experimental artifact due to the high variability in the results for this test condition and thus, the TGO200 data point is not shown in Figure 1 (see Table S4 for all data). For both green algae and cyanobacteria, the toxicity of GBNMs was determined by changes in chlorophyll *a* (Chl *a*) concentration, as an indicator of biomass, after a 96h exposure with the GBNMs at concentrations from 0 to 100 µg/mL. The Chl *a* extraction method used to assess algal toxicity was chosen to avoid artefacts that could arise if using optical based methods such as optical density measurements.[45] Based on the dose-response curves, the EC_{50} values for *M. aeruginosa* were 11.1 ± 2.36 for ARGO, 76.3 ± 12.6 for TGO200, and 126 ± 78.2 µg/mL for TGO500 (green circles). The EC_{50} value for TGO800 was not included in Figure 1 because the calculated value (45.5×10^3 µg/mL) was higher than any of the concentrations tested and therefore cannot be considered reliable. Similarly, for *S. obliquus*, only the EC_{50} value of ARGO could be calculated since, for all the TGO materials, there was no change in biomass at any of the tested concentrations (see Figure S1). The EC_{50} of ARGO for this species was calculated as 42.4 ± 15.1 µg/mL (Figure 1, purple dot). The absence of toxicity for the more reduced TGOs, compared to ARGO, does suggest a similar trend in *S. obliquus* as in *M. aeruginosa*: the reduction of ARGO to TGO reduces the toxicity of the material for both organisms.

The relationship between the C/O ratio of the different GBNMs and their toxicity to the different organisms is illustrated in Figure 1. For bacteria and invertebrates, the trend is similar, where the highest toxicity comes from the reduced materials and the lowest toxicity from ARGO. For both *E. coli* and *D. magna*, there is a strong linear relationship between reduction degree and toxicity with an $R^2 = 0.91$ for bacteria and an $R^2 = 0.99$ for invertebrates. Interestingly, for algae, the results show the opposite trend from those of *E. coli* and *D. magna*. Particularly, for *M. aeruginosa*, the strong ($R^2 = 0.97$) EC_{50}-C/O relationship shows that TGO500 (C/O = 7.61) is less toxic than ARGO (C/O = 2.01).

Overall, there are two main trends, one where the oxidized materials are less toxic than reduced materials and vice versa. These trends have been observed throughout in published literature.[23,27,46–52] In *E. coli*, for example, results agree with a previous study where a highly oxidized GO showed a 59% reduction in cell viability compared to 84% from rGO after 1h of exposure. This is attributed to a better charge transfer between the

bacteria and the sharper edges of the rGO. A similar trend is observed even in *S. aureus*, a Gram-positive bacterium but showed higher sensitivity than *E. coli*, with 74% cell viability loss in GO and 95% viability loss in rGO.[52] Similar results have been observed in *D. magna*, where the immobilization of daphnids after exposure to graphene and GO resulted in EC_{50} values of 31.62 ± 5.46 mg/L and 150 ± 19.4 mg/L.[53] Zhang et al. also reported that graphene functionalization alters algal cell viability. They reported differences in cell viability loss in *S. obliquus* after exposure to graphene, GO, and an amine-modified graphene yielding EC_{50} values of 8.2 mg/L, 20.6 mg/L, and 84.0 mg/L, respectively. Other studies, however, have shown the opposite trend, where GOs containing oxygen functional groups form more stable dispersions and offer more chances to interact with the cells, therefore exhibiting higher toxicity than rGO. Zhao et al. reported that GO and rGO materials with different extents of oxidation alter bacteria viability differently when exposed to 40 mg/L of the materials. The most oxidized GO was the most toxic and reduced viability by 41.2% whereas the rGO reduced it by 14.7%.[47] The differences in trends observed across previous studies can be attributed to two main factors even when testing the same organisms: the experimental conditions used and the type of materials. On one hand, many of the previous studies test the cell-material interactions at one arbitrary concentration or using different exposure times, making it difficult to correlate results across studies. On the other, material characterization (i.e., C/O ratio) is not usually reported (estimated in Table S1), which translates into trying to compare materials with very different properties.
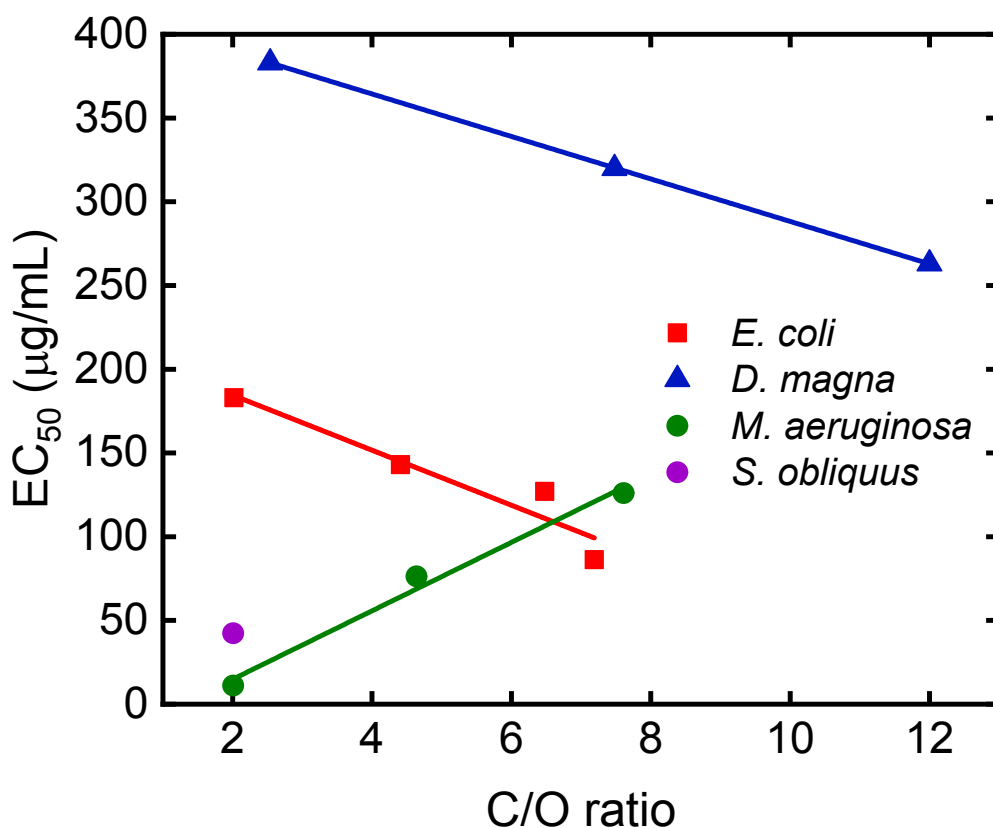

Figure 1. EC_{50} values of GBNMs of different C/O ratios for cyanobacteria (*M. aeruginosa*, 96h assay); green algae (*S. obliquus*, 96h assay); bacteria (*E. coli*, 3h assay), and invertebrates (*D. magna*, 48h assay). The exposure time is based on standard protocols for each model. The EC_{50} values of *S. obliquus* after a 96h contact time with the TGO materials could not be calculated as there was no response (Figure S1). Each point represents the average of three individual experiments with triplicate samples (n=9).

3.3 ARGO aggregation changes in different media. The influence of ionic strength and media components on nanomaterial aggregation is well documented and has been proposed as influencing NMs' toxicity.[54] To determine whether the observed EC_{50} trends are governed by aggregation, we monitored aggregation of ARGO in the different test media. Each biological media has a different ionic strength and composition (Table S4) [49], which can influence the GBNMs aggregation.[55–58] Since the EC_{50} is significantly different for the

different organisms (11.1 μg/mL for *M. aeruginosa* vs 383 μg/mL for *D. magna*), observing aggregation of ARGO in the different media will provide insight into its contribution to our observed trends. ARGO aggregation was analyzed at the beginning (5 min) and end of the toxicity assay durations (3h for bacteria, 48h for invertebrates, and 96h for algae) without organisms present. In addition to the EC_{50} concentration, changes in D_h were assessed at a constant ARGO concentration (100 μg/mL) to account for any concentration effects (Figure 2). Since determining D_h values by DLS and Stokes-Einstein equation assumes spherical particles, the values reported here are not representative of the real particle size since GO is not spherical. However, the change in D_h is an indicator of the relative GO aggregate size in the different media.[59]

When the ARGO concentration remained constant at 100 μg/mL, the initial D_h for BBM, 0.9% NaCl, and ISO were 0.13 ± 0.00, 0.58 ± 0.15, and 0.30 ± 0.04 μm respectively (solid bars) whereas the final were 0.26 ± 0.08, 0.80 ± 0.17, and 0.64 ± 0.18 μm (dashed bars) (Fig 2A). The 0.9% NaCl media used in the bacteria studies showed statistically significant differences in ARGO aggregate size compared to BBM and ISO ARGO aggregates (as D_h) in both initial and final measurements. The difference in aggregate size is attributable to the different ionic strengths and polyvalent cation composition and concentrations in the different media (Tables S5 and S6). ARGO has the largest aggregate size in 0.9% NaCl media, with the highest ionic strength (147.9 mM) compared to BBM or ISO media (7.10 and 6.74 mM, respectively). Moreover, the initial and final D_h values are statistically different for the BBM and ISO media. The change in aggregate size indicates that over time, the interaction between the aggregates and the organisms could change. These results suggest that the media composition differentially influences ARGO aggregation. Yet, 100 ug/mL is not representative of the ARGO concentration used in the respective toxicity assays and thus, does not capture the aggregation behavior of ARGO when in contact with the different organisms. We, therefore, also investigate the change in D_h at the respective EC_{50}.

When aggregation is considered at the same biologically relevant concentration, the EC_{50}, results show no statistical difference in ARGO D_h across media at the initial measurements, which range from 0.12 ± 0.04 μm to 0.23 ± 0.10 μm. However, when measured at the end of the exposure period for each organism, the D_h values increased to 0.21 ± 0.11, 0.42 ± 0.29, 0.66 ± 0.31, and 1.02 ± 0.61 μm for BBM (*M. aeruginosa, S. obliquus*), 0.9% NaCl (*E. Coli*), and ISO (*D. Magna*), respectively (Figure 2B). Only the D_h value at 96h in ISO medium is statistically different from the others and is explained by the higher concentration of polyvalent cations (Table S6), which are known to have a greater influence on the aggregation of GO.[55,60] Specifically, Ca^{2+} and Mg^{2+}, which tend to form cation bridges with carboxyl groups[60]. This complexation is supported by FTIR analysis on the materials after exposure to the media (Figure S3). Divalent electrolytes are known to be more effective at coagulating or destabilizing GO suspensions.[61] The different media also had a slight difference in pH, ranging from 6.8 to 7.8 (Table S6). However, this range remains biologically relevant and the difference in pH is not expected to play a major role in the difference in D_h between the media.[56]

Aggregation can alter the way GBNMs interact with the different organisms. For example, cell wrapping, which is a common mechanism observed in *E. coli*,[27,48,62] *S. obliquus*[7,50] and *M. aeruginosa*[50,63], would be affected by the decrease in available surface area caused by GO aggregation. This aligns with the results observed herein, as both species of algae experienced higher cytotoxicity (shown as lower EC_{50} values) than *E. coli*, while also having lower aggregate sizes over the duration of the study (Figure 2B). External GO accumulation has also been observed with *D. magna*, reducing the speed of motion.[64] While this is unlikely a direct factor in toxicity, the impact on motion could reduce survivability in the natural environment. Membrane damage and wall permeation is another commonly proposed mechanism that can be affected by aggregation, as the increased thickness of re-stacked GO can induce the nano-knife effect.[65] This mechanism is observed less in *M. aeruginosa* due to the presence of an adhesive external layer serving as protection.[50] Based upon the EC_{50} values and aggregate size results herein, *E. coli* and *S. obliquus* align with this mechanism. Internalization of the material via active uptake mechanisms will also be affected by the aggregate size. Although *Daphnia* can take in materials from 0.4-40 μm,[7,65] the rate of uptake is significantly reduced outside of 0.24-

0.64 μm.[53,66,67] Based on the aggregation observed in ISO medium, the rate of GO uptake in *D. magna* could significantly decrease throughout the study, reducing toxicity (as shown by the EC_{50} values in Figure 1). Other factors that impact material-organism interactions include the shape and facets of the materials before and after aggregation, which determine the surface area available, the sites available for interaction, charge to surface area ratio, and surface energy, as observed with other nanomaterials like MWCNTs[68], cuprous oxide[69] and silver[70], and in multiple organisms like bacteria, zebrafish[15,71], and algae[45].

Since all the different organisms considered had different physiology, growth cycle, and media requirements, it was impossible to use homogeneous testing conditions. As a result, the ARGO aggregation behavior is expected to be different in the different assay conditions. Overall, the changes in ARGO's aggregation behavior are attributed to electrostatic interactions between the oxygen functional groups present in the material and the monovalent and divalent ions present in each media. However, characterizing the aggregation behavior in each media is important to understand the potential importance of aggregation in toxicity under the assay conditions. Based on the results (Figure 2A), there is no clear relationship between D_h and EC_{50} when the same ARGO concentration is used. The medium that induced the highest aggregation, the 0.9% NaCl medium, did not have the highest EC_{50} value (Figure 2A). At the ARGO EC_{50}, the D_h increases as the EC_{50} increases; however, this may be also related to the higher GO concentrations in the test medium, which lead to larger aggregate size (Figures 2B and S2). Therefore, while aggregation may influence the toxicity of GBNMs, species-specific factors are likely to have a more important impact on the measured EC_{50}.
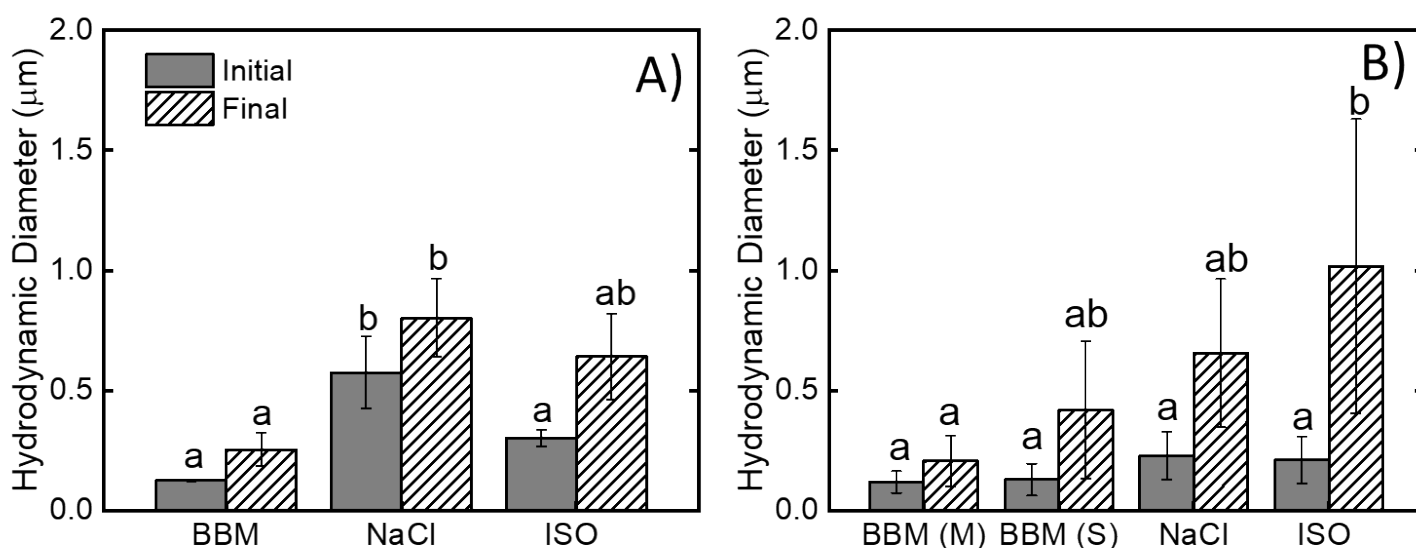

Figure 2. Hydrodynamic diameter (D_h) measurements for the initial (5 min) and final ARGO DLS measurements in 0.9% NaCl (3h), BBM (96h), and ISO (48h) for A) constant ARGO concentration of 100 ug/mL and B) EC_{50} ARGO concentration for *M. aeruginosa* (purple), *S. obliquus* (green), *E. coli* (red), and *D. magna* (blue). Solid and dashed bars represent initial and final DLS measurements, respectively. The letters in parenthesis in Fig 2B represent *M. aeruginosa* and *S. obliquus*, respectively since both algae used BBM media. Results are shown as average ± standard deviation (n=3). Different letters represent significant statistical differences (p≤ 0.05) across the different media.

3.4 Cellular response of bacteria and cyanobacteria to GBNMs. The relationship between C/O ratio and EC_{50} in GBNMs was found to differ between organisms. Among the four organisms tested in this study, *E. coli* and *M. aeruginosa* have the most contrasting results and display opposite trends in toxicity (see Fig. 1) despite being the most closely related organisms (both gram negative prokaryotic organisms). These findings highlight that the properties that make a material hazardous are not the same across species. To determine if these opposite trends are associated with a difference in how the materials interact with the cells, the response of each organism to oxidized (ARGO) and reduced ARGO (TGO500 or TGO800) was evaluated using fluorescent dye-based assays that probe different cellular responses characteristic of NMs exposure. The dyes used are fluorescein diacetate (FDA), and H2DCFDA, which evaluate esterase activity or reactive oxygen species (ROS) levels, respectively (Fig. 3A-B). The materials were compared at their EC_{50}

concentrations: 180 µg/mL for ARGO and 90 µg/mL TGO800 for *E. coli*; 11 µg/mL ARGO and 130 µg/mL TGO500 for *M. aeruginosa*. By comparing materials at their EC_{50} and not on a fixed nominal concentration, we integrate any effect of reduced bioavailability due to the differences in colloidal stability of the different materials in the different media to put the focus only on whether or not the same level of toxicity was induced by the same mechanisms in *E. coli* compared to *M. aeruginosa*. By taking this approach, the question changes from "which material is more toxic?" to "how is this toxicity induced?".

Although the exact toxicity mechanisms procured by GBNMs is still a matter of investigation, several effects have been proposed as possible pathways for GO's antimicrobial activity. These GO-organism interactions include two main mechanisms: 1) physical mechanisms like sheet adsorption on the cell membrane's surface or membrane puncturing and penetration through the lipid bilayer, and 2) chemical mechanisms like lipid extraction by the GO sheets and oxidative stress generation.[3] Dye results show that in bacteria, the toxicity of ARGO was characterized by a 55% increase in intracellular ROS while, for TGO800, no significant ROS production was observed. However, FDA fluorescence, which is associated with metabolic activity and membrane integrity, increased by 74% (Figure 3A). These results are in agreement with the higher biological reactivity typically observed in more oxidized GBNMs.[3,27,72] Conversely, for *M. aeruginosa*, ARGO decreased intracellular ROS and FDA fluorescence levels by 31% and 69%, respectively, when compared to control, while TGO800 only had a significant effect on FDA fluorescence, reducing it by 28% with respect to the control (Figure 3B). These results show a contrasting response of the two models to the different materials, where ARGO increases oxidative stress in bacteria but reduces it in cyanobacteria while TGOs increase metabolic activity in bacteria but reduces it in cyanobacteria. These results agree with the results obtained by the dose-response curves and the opposite trends observed in Figure 1, supporting the hypothesis that the interaction mechanisms between ARGO and bacteria are different from those observed with cyanobacteria. The same assays were performed without cells to confirm a lack of interferences coming from the dyes (Figure S4).

Previous studies have indicated that oxidative stress is an important mechanism of toxicity for GO in bacteria[27,48,73,74] and algae.[20,50,63,75,76] A rise of ROS production can cause damage to cellular components like proteins, lipids, and DNA.[77] Results show that ARGO, the most oxidized material in this study, has the highest potential of generating oxidative stress in bacteria compared to the thermally annealed TGOs. Previous studies have attributed this finding to the presence of reactive functional groups such as -OH and -COOH in the GO's surface, which are more likely to interact with biomolecules compared with rGO.[47] Additionally, Zhao et al. also demonstrated that the production of ROS by GO is linearly related to the oxidation degree of the material with R^2 values above 0.823, where GO with the highest oxygen content (58.6%) increased the ROS production because the oxygen functional groups transfer energy easier.[78,79] While CNMs have the capacity to directly generate ROS in a cellular environment or in the presence of light,[72,80] the increase in H_2DCFDA fluorescence may also be the result of an impact of ARGO exposure on the cell functions. In the cells, ROS are generated intracellularly during aerobiosis-fueled oxygen metabolism which generates superoxide ($O_2^{•-}$), hydrogen peroxide (H_2O_2), and highly destructive hydroxyl radicals ($OH^•$).[81] The fluorescent dye H_2DCFDA however, is a general stress indicator and is sensitive to a wide range of ROS and as such, this method only provides information regarding a generalized quantification of ROS.

Even though cyanobacteria do not show an increase in H_2DCFDA fluorescence, it is worth mentioning that the dye's fluorescent response is dependent on the esterase enzymes, which hydrolyze H_2DCFDA. Thus, since there is a decrease in FDA fluorescence, which is related to esterase enzymes activity, the H_2DCFDA response may be affected.[82] FDA is a nonfluorescent molecule that is taken up by cells by passive diffusion to be hydrolyzed by the esterase enzymes into the fluorescent fluorescein molecule. As such, FDA fluorescence is dependent on both the esterase enzyme activity and the integrity of the cell membrane.[83] The increase in FDA fluorescence in bacterial cells is attributed to an increase in the interactions between GO and the cells' surface[27,84] leading to a decrease in cell permeability causing dye retention. In the case of a decrease in FDA, as is observed with *M. aeruginosa*, the response suggests a decrease in metabolic activity associated with reduced photosynthesis or a disruption of the membrane integrity.[32] Previous studies have indicated that a light-shading effect induced by CNMs in

photosynthetic organisms may reduce photosynthetic activity without inducing oxidative stress.[45,85] This physical effect induced by GO on *M. aeruginosa* could explain the discrepancy observed for the effect of GBNMs between *E. coli*, which is non-photosynthetic, and *M. aeruginosa*.

Given the potential influence of esterase activity on the measured ROS level, the H_2DCFDA results were corroborated with a second assay, the measure of the intracellular catalase (CAT) activity (Fig. 3C-D). The CAT enzyme, along with superoxide dismutase (SOD), ascorbate peroxidase (APOX), and low molecular weight antioxidants (i.e., glutathione), constitute the antioxidant defense system developed by all organisms to protect themselves against ROS damage.[86,87] The CAT enzyme activity was chosen here as an indicator of oxidative stress because previous studies have shown that CAT is a more sensitive indicator of oxidative stress induced by NMs compared to the other enzymes.[39,88] The CAT enzyme dismutates H_2O_2 as given by the reaction below, where H_2O_2 is converted to water and oxygen:[87]

$$2H_2O_2 \rightarrow 2H_2O + O_2$$
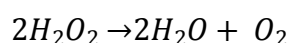
Results show that in bacteria exposed to ARGO, there is a significant increase in CAT activity from 15.3 ± 4.13 mmol/min$^{-1} \cdot \mu g^{-1}$ in the control treatment to 52.4 ± 7.36 mmol/min$^{-1} \cdot \mu g^{-1}$ in ARGO treated bacterial cells (Fig. 3C). Additionally, there was no statistical difference between control and TGO800 treated cells. For cyanobacteria, cells treated with ARGO or TGO500 showed no difference in CAT activity when compared to controls (Fig. 3D). These results agree with the observations made with the fluorescent dyes and confirm that ARGO, the most oxidized material, induces the highest oxidative stress level in bacterial cells, thus evidencing a chemical mechanism of action. Likewise, catalase results in cyanobacteria confirm that oxidative stress is not a primary mechanism taking place between the GBNMs and the cells, perhaps showcasing a physical mechanism of action. Therefore, the two organisms show a clear difference in how they respond to change in oxygen content when exposed to GBNMs. The assays were done in the same conditions but without the addition of cells to confirm that the materials did not interfere with the observed responses. Due to a lack of catalase source (no organisms), no H_2O_2 decomposition was observed (Figure S5 and Table S7).
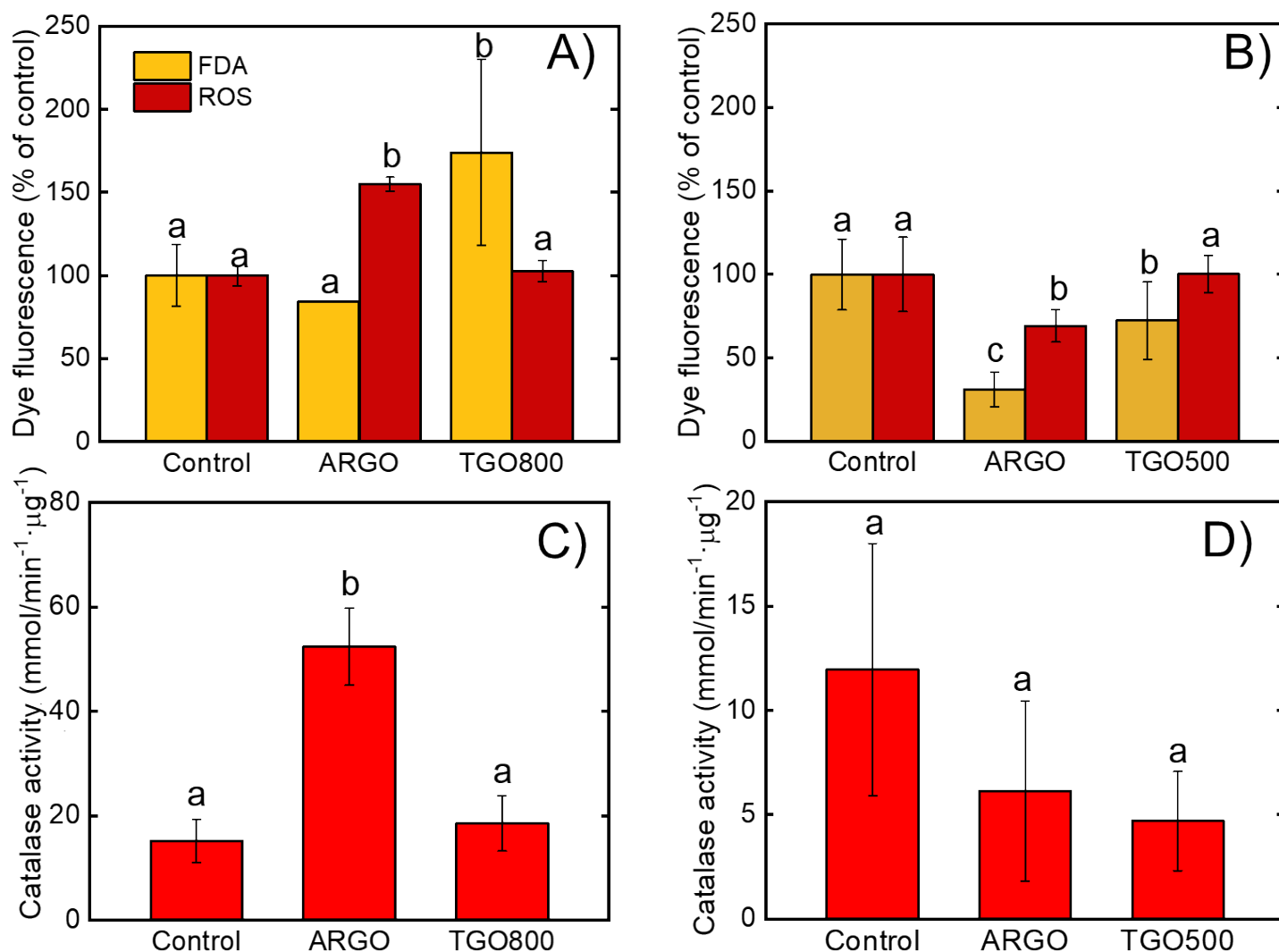
Figure 3. Biochemical responses of ARGO and TGOs in *E. coli* and *M. aeruginosa* after 3h and 96h of exposure at their EC_{50} concentrations, respectively. Top panels are fluorescent dye assays showing esterase activity and reactive oxygen species generation for A) *E. coli* and B) *M. aeruginosa*. Data was normalized to the fluorescence response of the control. Bottom panels show catalase activity for C) *E. coli* and D) *M. aeruginosa*. Negative controls using only media (0.9% NaCl or BBM) and bacteria or algae were used throughout (no GO). Different letters represent significant statistical differences ($p \leq 0.05$) compared to the control (n=9).

3.5 Effect of GBNMs on cellular integrity. Since membrane damage is often associated with the toxicity of GBNMs in microorganisms, changes induced by GBNMs exposure to the cellular structure or morphology were evaluated using electron microscopy (Figure 4). Cell morphology was evaluated by SEM (Fig. 4A-F) and TEM (Fig. 4G-I) for *E. coli* and *M. aeruginosa* after exposure to the EC_{50} concentrations of ARGO and TGOs for 3h and 96h, respectively. Figure 4A shows an SEM micrograph of *E. coli* cells not treated with NMs. They appear healthy and with their characteristic rod shape. After exposure to ARGO, however, over 90% of the cells are covered by the material. ARGO appears quite "fibrous" and seem to wrap around the bacterial cells (Fig. 4B). TGO800 sheets encounter aggregates of bacterial cells with only about 23% coming in contact with the material and no evidence of damage as observed in Fig. 4C.

The SEM micrograph in Fig. 4D shows control cyanobacterial cells as round and plump. Upon exposure to ARGO, over 98% of *M. aeruginosa* cells appear to have a "velvet" or wrinkled texture due to a layer of ARGO deposited on the cells' surface (Fig. 4E). All the cells have a similar wrinkled surface which indicates that ARGO interacts with cyanobacteria in a uniform manner. Conversely, cyanobacterial cells exposed to TGO500

show that the cells appear to be in contact with large TGO500 aggregates, and not covered by the material (Fig. 4F). For both materials, however, the cells-material interactions do not seem to alter the cells' overall structure; they retain their shape, and no indication of membrane damage is evidenced. Similar results were observed in a study by Tang et al. where *M. aeruginosa* was exposed to GO and SEM imaging showed GO adhesion onto the cells' surface and no morphological changes.[63] Other studies show internalization of GO in algal cells,[63,89] however, that is not the case in our conditions.

The effect of GBNMs on bacteria and cyanobacteria were further investigated by TEM imaging. The ultrastructure of *E. coli* cells after exposure to no NMs, ARGO, or TGO800 are shown in Fig. 4G-I. Untreated cells (Fig. 4G and insert) have smooth and regular cell walls, with homogeneous cytoplasmic contents. However, treated cells with ARGO are evidently surrounded by the material (Fig. 4H), unlike TGO800, where cells come in contact with aggregates of the material (Fig. 4I). Even though no evident physical disruption is observed, some cells look elongated with an average length of 1.38 ± 0.66 μm compared to the control (1.12 ± 0.42 μm) , especially after ARGO exposure (1.66 ± 0.58 μm). These results indicate that GO sheets could wrap around the bacteria cells, which has been observed in previous studies.[27,90] The wrapping mechanism occurring between ARGO and *E. coli* cells may help explain the oxidative stress response observed. Although there is a significant increase in ROS and catalase activity, electron microscopy images show no major damage in cell morphology or cellular components. To this point, previous reports have shown that the wrapping mechanism can isolate bacteria from their environment, thus, limiting access to nutrients and preventing their growth but without immediate cell inactivation.[90] Therefore, an oxidative response may have been triggered without resulting yet to an oxidative damage to the membrane.

As shown in TEM images, most *M. aeruginosa* cells have intact cell membranes after exposure to both materials with a few exceptions (Fig. 4J-L, and inserts). Control cells (Fig. 4J and insert) have a normal intracellular structure with a three-layer cell wall, dense cytoplasm, and had the typical organelles: cyanophycin granules, lipid droplets, polyphosphate bodies, thylakoid, and ribosome clearly visible.[91] In contrast, cyanobacterial cells exposed to either ARGO or TGO500 show a less defined ultrastructure, with large vacuoles localized in the cell, and an overall smaller cell size (more noticeable with TGO500 with an average length of 1.29 ± 0.54 μm) when compared to untreated cells (1.83 ± 0.66 μm). For ARGO, the majority of the cells (>90%) are surrounded by the material (like in SEM images and Fig. 4K), while for TGO500, the material appears to be concentrated as an aggregate (Fig. 4L). These results suggest that the reduction in FDA fluorescence is not due to membrane damage and that a lower metabolic activity may be involved. When exposed to CNMs, photosynthetic organisms were shown to experience lower photosynthetic activity due to a shading effect caused by the dark GBNMs in the medium and around the cells. Photosynthesis being the only source of cellular energy for cell division and growth, the shading effect could lead to a decrease metabolic activity and lower FDA fluorescence.[92] These observations agree with other reports where photosynthetic organisms were exposed to GBNMs.[85]

For both *M. aeruginosa* and *E. coli*, the cells do not appear to have the collapsed structure indicative of membrane disruption and cell damage observed in previous studies involving the interactions of bacteria with GBNMs.[73] This contrast may be attributed to species-specific differences like the different cell wall architecture between bacteria and cyanobacteria, where *M. aeruginosa* cell walls have a thicker peptidoglycan layer that can offer additional protection against membrane damage.[93]
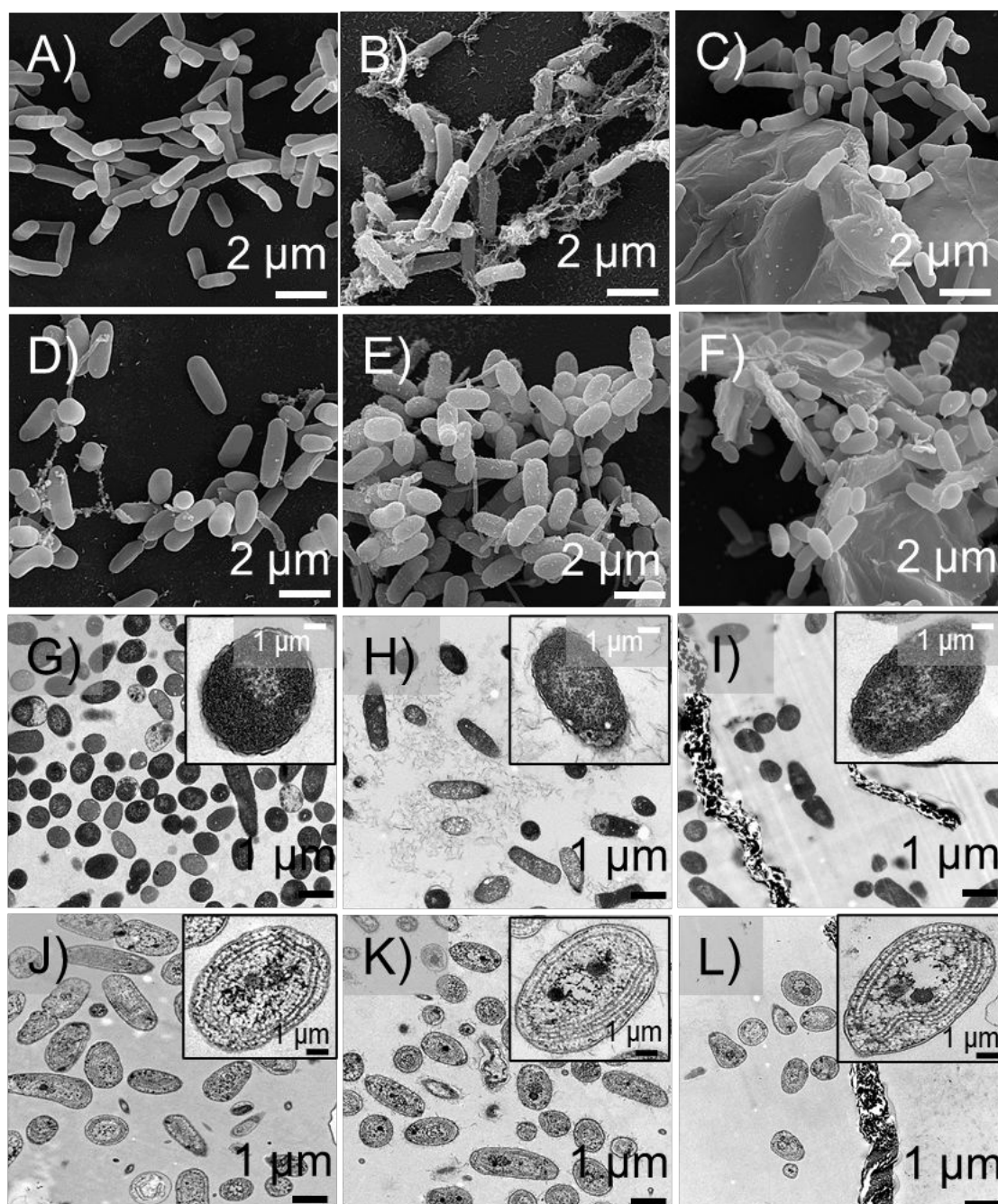
Figure 4. Scanning electron micrographs (A-F) and transmission electron micrographs (G-L) of *E. coli* and *M. aeruginosa* cells with and without GBNMs. First and third panels show *E. coli* cells with no GO (A, G); cells exposed to the ARGO EC_{50} concentration (B, H); and cells exposed to the TGO800 EC_{50} concentration (C, I) for 3h. Second and fourth panels show *M. aeruginosa* cells with no GO (D, J); cells exposed to the ARGO EC_{50} concentration (E, K); and cells exposed to the TGO500 EC_{50} concentration for 96h. Inserts in G-L are enlarged pictures of cells representative of the interaction observed.

4. Conclusions

Environmental risk assessment requires knowledge of GBNMs toxicity on different trophic levels. Yet current studies primarily focus on a single organism within one taxon. Our study contributes to the current body of knowledge on GBNM toxicity by using the same materials studied in multiple organisms across 3 taxa as well as focuses on the influence of surface chemistry (C/O ratio, specifically) on observed toxicity impacts. The present study, conducted on bacteria, photosynthetic microorganisms, and invertebrates provides valuable information on the individual response to different organisms to a suite of systematically reduced GO materials. Findings show that the properties that make a material hazardous are not the same across species. Overall, results show that photosynthetic organisms have a higher sensitivity towards ARGO compared to bacteria and invertebrates as observed by lower EC_{50} values. Thermal annealing of the material reduced the toxicity in photosynthetic organisms but increased it in bacteria and

18

invertebrates. These opposing trends between toxicity and oxygen content were investigated using *M. aeruginosa* and *E. coli* and clear differences in the mechanisms of interactions were found for the different materials in these two biological models. On one hand, the toxicity of the GBNMs towards *M. aeruginosa* was characterized by a decrease in overall cellular metabolic activity, thus, proposing a physical mechanism of action due to close contact between ARGO and the cells, while in *E. coli*, ARGO induced significant oxidative stress, evidenced by both H_2DCFDA fluorescence and CAT enzyme activity, elucidating a chemical mechanism of action. It is worth noting that the results found in this study are not meant to provide a fit-for-all answer for every organism-material interaction in each taxon, meaning not all bacteria, algae, or invertebrate species will have the same responses as those observed with the organisms in this study. Rather, these findings emphasize how different surface chemistries and species-specific parameters alter the toxicity of GBNMs and highlight the need to consider the specific response of each organism when developing safe-by-design guidelines for GBNMs, as different organisms will respond differently to changes in the materials' properties. This study then, warns us that applying broadly safe design guidelines across species can lead to an unwanted increase in hazard if the structure-property-toxicity relationships of the material are not well understood.

Supporting Information: Dose-response curves of *S. obliquus* after a 96h exposure with ARGO or TGOs (Figure S1); Relationship between GBNMs' hydrodynamic diameter and EC_{50} in each media (Figure S2); Fourier transform infrared spectrometry of ARGO and TGO8000 (Figure S3); Fluorescence intensity of FDA and H_2DCFDA dyes over a 3h period without the addition of cells (Figure S4); Absorbance intensity at 240 nm to assess H_2O_2 decomposition without the addition of cells (Figure S5); Compiled literature comparing graphene-based nanomaterials and different species (Table S1); XPS data representing the atomic percent of carbon and oxygen content, and carbon-oxygen functional groups (Table S2); XPS data representing trace impurities in GBNMs (Table S3); Immobilization responses of *D. manga* after exposure to GBNMs (Table S4); Chemical composition and concentrations for the preparations of 0.9% NaCl, ISO, and BBM medias (Table S5); Solution chemistry characteristics of the different media: BBM, 0.9% NaCl, and ISO (Table S6); Intercepts and slopes of each linear fit according to the H_2O_2 decomposition over 3 minutes. This material is available free of charge.

CRediT author statement

A.C. Barrios: Conceptualization, Supervision, Investigation, Validation, Visualization, Writing- Original draft preparation, Writing- Reviewing and Editing.

Y.P. Cahue: Investigation, Validation, Writing- Reviewing and Editing.

Y. Wang: Conceptualization, Supervision, Investigation, Validation, Visualization, Writing- Reviewing and Editing.

J. Geiger: Conceptualization, Investigation, Validation, Writing- Original draft preparation, Writing- Reviewing and Editing.

R.C. Puerari: Conceptualization, Investigation, Validation, Visualization, Writing – Original draft preparation, Writing- Reviewing and Editing.

W.G. Matias: Conceptualization, Writing- Reviewing and Editing.

S.P. Melegari: Conceptualization, Writing- Reviewing and Editing.

L.M. Gilbertson: Conceptualization, Supervision, Funding acquisition, Writing- Original draft preparation, Writing- Reviewing and Editing.

F. Perreault: Conceptualization, Supervision, Funding acquisition, Writing- Original draft preparation, Writing- Reviewing and Editing.

References:

1   Y. Zhang, T. R. Nayak, H. Hong and W. Cai, Graphene: A versatile nanoplatform for biomedical applications, *Nanoscale*, 2012, **4**, 3833–3842.

2   Y. Huang, J. Liang and Y. Chen, An overview of the applications of graphene-based materials in supercapacitors, *Small*, 2012, **8**, 1805–1834.

3   F. Perreault, A. F. de Faria and M. Elimelech, Environmental applications of graphene-based nanomaterials, *Chem. Soc. Rev.*, 2015, **44**, 5681–5896.

4   Report, *Graphene Market Size, Share & Trends Analysis Report By Application (Electronics, Composites, Energy), By Product (Graphene Nanoplatelets, Graphene Oxide), By Region, And Segment Forecasts, 2020 - 2027*, 2020, vol. 2027.

5   D. R. Dreyer, S. Park, C. W. Bielawski and R. S. Ruoff, The chemistry of graphene oxide, *Chem. Soc. Rev.*, 2010, **39**, 228–240.

6   A. Bianco, H. M. Cheng, T. Enoki, Y. Gogotsi, R. H. Hurt, N. Koratkar, T. Kyotani, M. Monthioux, C. R. Park, J. M. D. Tascon and J. Zhang, All in the graphene family - A recommended nomenclature for two-dimensional carbon materials, *Carbon N. Y.*, 2013, **65**, 1–6.

7   Y. Zhang, T. Meng, L. Shi, X. Guo, X. Si, R. Yang and X. Quan, The effects of humic acid on the toxicity of graphene oxide to Scenedesmus obliquus and Daphnia magna, *Sci. Total Environ.*, 2019, **649**, 163–171.

8   Y. Wang and L. M. Gilbertson, Informing rational design of graphene oxide through surface chemistry manipulations: Properties governing electrochemical and biological activities, *Green Chem.*, 2017, **19**, 2826–2838.

9   A. B. Seabra, A. J. Paula, R. De Lima, O. L. Alves and N. Durán, Nanotoxicity of graphene and graphene oxide, *Chem. Res. Toxicol.*, 2014, **27**, 159–168.

10   H. E. Karahan, L. Wei, K. Goh, Z. Liu, Ö. Birer, F. Dehghani, C. Xu, J. Wei and Y. Chen, Bacterial physiology is a key modulator of the antibacterial activity of graphene oxide, *Nanoscale*, 2016, **8**, 17181–17189.

11   X. Lu, X. Feng, J. R. Werber, C. Chu, I. Zucker, J.-H. H. Kim, C. O. Osuji and M. Elimelech, Enhanced antibacterial activity through the controlled alignment of graphene oxide nanosheets, *Proc. Natl. Acad. Sci.*, 2017, **114**, E9793–E9801.

12   H. N. Nguyen, S. L. Castro-Wallace and D. F. Rodrigues, Acute toxicity of graphene nanoplatelets on biological wastewater treatment process, *Environ. Sci. Nano*, 2017, **4**, 160–169.

13   C. Hu, Q. Wang, H. Zhao, L. Wang, S. Guo and X. Li, Ecotoxicological effects of graphene oxide on the protozoan Euglena gracilis, *Chemosphere*, 2015, **128**, 184–190.

14   T. Mesarič, K. Sepčič, V. Piazza, C. Gambardella, F. Garaventa, D. Drobne and M. Faimali, Effects of nano carbon black and single-layer graphene oxide on settlement, survival and swimming behaviour of Amphibalanus amphitrite larvae, *Chem. Ecol.*, 2013, **29**, 643–652.

15   M. Chen, J. Yin, Y. Liang, S. Yuan, F. Wang, M. Song and H. Wang, Oxidative stress and immunotoxicity induced by graphene oxide in zebrafish, *Aquat.*

Toxicol., 2016, **174**, 54–60.

16   X. Yang, Q. Yang, G. Zheng, S. Han, F. Zhao, Q. Hu and Z. Fu, Developmental
         neurotoxicity and immunotoxicity induced by graphene oxide in zebrafish
         embryos, *Environ. Toxicol.*, 2019, **34**, 415–423.

17   H. Li, F. Cao, F. Zhao, Y. Yang, M. Teng, C. Wang and L. Qiu, Chemosphere
         Developmental toxicity , oxidative stress and immunotoxicity induced by three
         strobilurins (pyraclostrobin , tri fl oxystrobin and picoxystrobin) in zebra fi sh
         embryos, *Chemosphere*, 2018, **207**, 781–790.

18   B. Khan, A. S. Adeleye, R. M. Burgess, S. M. Russo and K. T. Ho, Effects of
         graphene oxide nanomaterial exposures on the marine bivalve, Crassostrea
         virginica, *Aquat. Toxicol.*, 2019, **216**, 105297.

19   B. Khan, A. S. Adeleye, R. M. Burgess, R. Smolowitz, S. M. Russo and K. T. Ho,
         A 72-h exposure study with eastern oysters (Crassostrea virginica) and the
         nanomaterial graphene oxide, *Environ. Toxicol. Chem.*, 2019, **38**, 820–830.

20   S. Du, P. Zhang, R. Zhang, Q. Lu, L. Liu, X. Bao and H. Liu, Reduced graphene
         oxide induces cytotoxicity and inhibits photosynthetic performance of the green
         alga Scenedesmus obliquus, *Chemosphere*, 2016, **164**, 499–507.

21   S. Loureiro, S. Filipe, G. Gonçalves, M. Jesús, S. Rebelo, M. Carmona and M.
         Vila, Ecotoxicology and Environmental Safety Eco-friendly pro fi le of pegylated
         nano-graphene oxide at di ff erent levels of an aquatic trophic chain, *Ecotoxicol.
         Environ. Saf.*, 2018, **162**, 192–200.

22   X. Lv, Y. Yang, Y. Tao, Y. Jiang, B. Chen, X. Zhu, Z. Cai and B. Li, A
         mechanism study on toxicity of graphene oxide to Daphnia magna : Direct link
         between bioaccumulation and oxidative stress * , **, *Environ. Pollut.*, 2018, **234**,
         953–959.

23   Y. Liu, W. Han, Z. Xu, W. Fan, W. Peng and S. Luo, Comparative toxicity of
         pristine graphene oxide and its carboxyl , imidazole or polyethylene glycol
         functionalized products to Daphnia magna : A two generation study *, *Environ.
         Pollut.*, 2018, **237**, 218–227.

24   A. Al-Jumaili, S. Alancherry, K. Bazaka and M. V. Jacob, Review on the
         antimicrobial properties of Carbon nanostructures, *Materials (Basel).*, 2017, **10**, 1–
         26.

25   M. D. Rojas-Andrade, G. Chata, D. Rouholiman, J. Liu, C. Saltikov and S. Chen,
         Antibacterial mechanisms of graphene-based composite nanomaterials, *Nanoscale*,
         2017, **9**, 994–1006.

26   L. M. Gilbertson, J. B. Zimmerman, D. L. Plata, J. E. Hutchison and P. T. Anastas,
         Designing nanomaterials to maximize performance and minimize undesirable
         implications guided by the Principles of Green Chemistry, *Chem. Soc. Rev.*, 2015,
         44, 5758–5777.

27   A. C. Barrios, Y. Wang, L. M. Gilbertson and F. Perreault, Structure − Property −
         Toxicity Relationships of Graphene Oxide : Role of Surface Chemistry on the
         Mechanisms of Interaction with Bacteria, *Environ. Sci. Technol.*, 2019, **53**, 14679–
         14687.

28   L. M. Gilbertson, D. G. Goodwin, A. D. Taylor, L. Pfefferle and J. B. Zimmerman,
         Toward tailored functional design of multi-walled carbon nanotubes (MWNTs):
         Electrochemical and antimicrobial activity enhancement via oxidation and
         selective reduction, *Environ. Sci. Technol.*, , DOI:10.1021/es500468y.

29   H. Enis Karahan, Y. Wang, W. Li, F. Liu, L. Wang, X. Sui, M. A. Riaz and Y.
         Chen, Antimicrobial graphene materials: The interplay of complex materials
         characteristics and competing mechanisms, *Biomater. Sci.*, 2018, **6**, 766–773.

30   A. R. Deline, B. P. Frank, C. L. Smith, L. R. Sigmon, A. N. Wallace, M. J.
         Gallagher, D. G. Goodwin, D. P. Durkin and D. Howard Fairbrother, Influence of
         oxygen-containing functional groups on the environmental properties,
         transformations, and toxicity of carbon nanotubes, *Chem. Rev.*, 2020, **120**, 11651–
         11697.

31   L. M. Pasquini, R. C. Sekol, A. D. Taylor, L. D. Pfefferle and J. B. Zimmerman, Realizing comparable oxidative and cytotoxic potential of single- and multiwalled carbon nanotubes through annealing, *Environ. Sci. Technol.*, 2013, **47**, 8775–8783.

32   P. Radix, M. Léonard, C. Papantoniou, G. Roman, E. Saouter, S. Gallotti-Schmitt, H. Thiébaud and P. Vasseur, Comparison of four chronic toxicity tests using algae, bacteria, and invertebrates assessed with sixteen chemicals, *Ecotoxicol. Environ. Saf.*, 2000, **47**, 186–194.

33   A. Chalifour, A. LeBlanc, L. Sleno and P. Juneau, Sensitivity of Scenedesmus obliquus and Microcystis aeruginosa to atrazine: effects of acclimation and mixed cultures, and their removal ability, *Ecotoxicology*, 2016, **25**, 1822–1831.

34   H. K. Lichtenthaler, Chlorophylls Carotenoids, *Chlorophylls Carotenoids Pigment. Photosynth. Biomembr.*, 1987, **148**, 350–382.

35   ISO 6341, INTERNATIONAL STANDARD ISO inhibition of the mobility of Daphnia, 2012, **6341**, 11.

36   ABNT NBR 12713, Ecotoxicologia aquática — Toxicidade aguda — Método de ensaio com Daphnia spp (Crustacea, Cladocera) Aquatic, *Assoc. Bras. Normas Técnicas*, 2016, **4º Edição**, 1–23.

37   Z. Chen, R. Bertin and G. Froldi, EC50 estimation of antioxidant activity in DPPH* assay using several statistical programs, *Food Chem.*, 2013, **138**, 414–420.

38   M. A. Hamilton, R. C. Russo and R. V Thurston, Trimmed Spearman-Karber Method for Estimating Median Lethal Concentrations in Toxicity Bioassays, 1975, **566**, 714–719.

39   S. P. Melegari, F. Perreault, R. H. R. Costa, R. Popovic and W. G. Matias, Evaluation of toxicity and oxidative stress induced by copper oxide nanoparticles in the green alga Chlamydomonas reinhardtii, *Aquat. Toxicol.*, 2013, **142–143**, 431–440.

40   H. Aebi, Catalase in Vitro, *Methods Enzymol.*, 1984, **105**, 121–126.

41   E. Ann Ellis, Solutions to the Problem of Substitution of ERL 4221 for Vinyl Cyclohexene Dioxide in Spurr Low Viscosity Embedding Formulations, *Micros. Today*, 2006, **14**, 32–33.

42   N. Hanaichi, T., Sato, T., Iwamoto, T., Malavasi-Yamashiro, J., Hoshing, M., Mizuno, A stable lead by modification of Sato's method, *J. Electron Microsc. (Tokyo).*, 1986, **35**, 304–306.

43   H. L. Poh, F. Šaněk, A. Ambrosi, G. Zhao, Z. Sofer and M. Pumera, Graphenes prepared by Staudenmaier, Hofmann and Hummers methods with consequent thermal exfoliation exhibit very different electrochemical properties, *Nanoscale*, 2012, **4**, 3515–3522.

44   A. Ganguly, S. Sharma, P. Papakonstantinou and J. Hamilton, Probing the thermal deoxygenation of graphene oxide using high-resolution in situ X-ray-based spectroscopies, *J. Phys. Chem. C*, 2011, **115**, 17009–17019.

45   E. Cruces, A. C. Barrios, Y. P. Cahue, B. Januszewski, L. M. Gilbertson and F. Perreault, Similar toxicity mechanisms between graphene oxide and oxidized multi-walled carbon nanotubes in Microcystis aeruginosa, *Chemosphere*, 2021, **265**, 129137.

46   W. Hu, C. Peng, W. Luo, M. Lv, X. Li, D. Li, Q. Huang and C. Fan, Graphene-based antibacterial paper, *ACS Nano*, 2010, **4**, 4317–4323.

47   F. fei Zhao, S. chun Wang, Z. lin Zhu, S. guang Wang, F. fei Liu and G. zhou Liu, Effects of oxidation degree on photo-transformation and the resulting toxicity of graphene oxide in aqueous environment, *Environ. Pollut.*, 2019, **249**, 1106–1114.

48   M. Hofmann, J. Wei, Y. Chen, S. Liu, T. H. Zeng, M. Hofmann, E. Burcombe, J. Wei and R. Jiang, Antibacterial Activity of Graphite , Graphite Oxide , Graphene Oxide , and Reduced Graphene Oxide : Membrane and Oxidative Stress, 2011, 6971–6980.

49   Y. Tu, M. Lv, P. Xiu, T. Huynh, M. Zhang, M. Castelli, Z. Liu, Q. Huang, C. Fan,

H. Fang and R. Zhou, Destructive extraction of phospholipids from Escherichia coli membranes by graphene nanosheets, *Nat. Nanotechnol.*, 2013, **8**, 594–601.

50   J. Yin, W. Fan, J. Du, W. Feng, Z. Dong, Y. Liu and T. Zhou, The toxicity of graphene oxide affected by algal physiological characteristics: A comparative study in cyanobacterial, green algae, diatom, *Environ. Pollut.*, 2020, **260**, 113847.

51   K. Xu, H. Jiang, P. Juneau and B. Qiu, Comparative studies on the photosynthetic responses of three freshwater phytoplankton species to temperature and light regimes, *J. Appl. Phycol.*, 2012, **24**, 1113–1122.

52   O. Akhavan and E. Ghaderi, Toxicity of Graphene and Graphene Oxide Nanowalls Against Bacteria, 2010, **4**, 5731–5736.

53   Y. Liu, W. Fan, Z. Xu, W. Peng and S. Luo, Comparative effects of graphene and graphene oxide on copper toxicity to Daphnia magna: Role of surface oxygenic functional groups, *Environ. Pollut.*, 2018, **236**, 962–970.

54   M. Baalousha, Effect of nanomaterial and media physicochemical properties on nanomaterial aggregation kinetics, *NanoImpact*, 2017, **6**, 55–68.

55   I. Chowdhury, N. D. Mansukhani, L. M. Guiney, M. C. Hersam and D. Bouchard, Aggregation and Stability of Reduced Graphene Oxide: Complex Roles of Divalent Cations, pH, and Natural Organic Matter, *Environ. Sci. Technol.*, 2015, **49**, 10886–10893.

56   N. Ye, Z. Wang, S. Wang, H. Fang and D. Wang, Aqueous aggregation and stability of graphene nanoplatelets, graphene oxide, and reduced graphene oxide in simulated natural environmental conditions: complex roles of surface and solution chemistry, *Environ. Sci. Pollut. Res.*, 2018, **25**, 10956–10965.

57   K. Yang, B. Chen, X. Zhu and B. Xing, Aggregation, Adsorption, and Morphological Transformation of Graphene Oxide in Aqueous Solutions Containing Different Metal Cations, *Environ. Sci. Technol.*, 2016, **50**, 11066–11075.

58   M. Wang, Y. Niu, J. Zhou, H. Wen, Z. Zhang, D. Luo, D. Gao, J. Yang, D. Liang and Y. Li, The dispersion and aggregation of graphene oxide in aqueous media, *Nanoscale*, 2016, **8**, 14587–14592.

59   S. D. Story, S. Boggs, L. M. Guiney, M. Ramesh, M. C. Hersam, C. J. Brinker and S. L. Walker, Aggregation morphology of planar engineered nanomaterials, *J. Colloid Interface Sci.*, 2020, **561**, 849–853.

60   Y. Jiang, R. Raliya, J. D. Fortner and P. Biswas, Graphene Oxides in Water: Correlating Morphology and Surface Chemistry with Aggregation Behavior, *Environ. Sci. Technol.*, 2016, **50**, 6964–6973.

61   L. Wu, L. Liu, B. Gao, R. Muñoz-Carpena, M. Zhang, H. Chen, Z. Zhou and H. Wang, Aggregation kinetics of graphene oxides in aqueous solutions: Experiments, mechanisms, and modeling, *Langmuir*, 2013, **29**, 15174–15181.

62   J. Zhao, Z. Wang, J. C. White and B. Xing, Graphene in the Aquatic Environment: Adsorption, Dispersion, Toxicity and Transformation, *Environ. Sci. Technol.*, 2014, **48**, 9995–10009.

63   Y. Tang, J. Tian, S. Li, C. Xue, Z. Xue, D. Yin and S. Yu, Combined effects of graphene oxide and Cd on the photosynthetic capacity and survival of Microcystis aeruginosa, *Sci. Total Environ.*, 2015, **532**, 154–161.

64   A. M. Cano, J. D. Maul, M. Saed, S. A. Shah, M. J. Green and J. E. Cañas-Carrell, Bioaccumulation, stress, and swimming impairment in Daphnia magna exposed to multiwalled carbon nanotubes, graphene, and graphene oxide, *Environ. Toxicol. Chem.*, 2017, **36**, 2199–2204.

65   A. Baun, N. B. Hartmann, K. Grieger and K. O. Kusk, Ecotoxicity of engineered nanoparticles to aquatic invertebrates: A brief review and recommendations for future toxicity testing, *Ecotoxicology*, 2008, **17**, 387–395.

66   L. M. Skjolding, K. Kern, R. Hjorth, N. Hartmann, S. Overgaard, G. Ma, J. G. C. Veinot and A. Baun, Uptake and depuration of gold nanoparticles in Daphnia magna, *Ecotoxicology*, 2014, **23**, 1172–1183.

67 F. R. Khan, G. M. Kennaway, M. N. Croteau, A. Dybowska, B. D. Smith, A. J. A. Nogueira, P. S. Rainbow, S. N. Luoma and E. Valsami-Jones, In vivo retention of ingested au NPs by daphnia magna: No evidence for trans-epithelial alimentary uptake, *Chemosphere*, 2014, **100**, 97–104.

68 M. M. Falinski, M. A. Garland, S. M. Hashmi, R. L.Tanguay and J. B. Zimmerman, Establishing structure-property-hazard relationships for multi-walled carbon nanotubes: The role of aggregation, surface charge, and oxidative stress on embryonic zebrafish mortality, *Carbon N. Y.*, 2019, **155**, 587–600.

69 Y. Feng, Y. Chang, X. Sun, N. Liu, Y. Cheng, Y. Feng, H. Zhang and X. Li, Understanding the property-activity relationships of polyhedral cuprous oxide nanocrystals in terms of reactive crystallographic facets, *Toxicol. Sci.*, 2017, **156**, 480–491.

70 X. Wang, H. F. Wu, Q. Kuang, R. Bin Huang, Z. X. Xie and L. S. Zheng, Shape-dependent antibacterial activities of Ag2O polyhedral particles, *Langmuir*, 2010, **26**, 2774–2778.

71 Z. Chen, C. Yu, I. A. Khan, Y. Tang, S. Liu and M. Yang, Toxic effects of different-sized graphene oxide particles on zebrafish embryonic development, *Ecotoxicol. Environ. Saf.*, , DOI:10.1016/j.ecoenv.2020.110608.

72 X. Liu, S. Sen, J. Liu, I. Kulaots, D. Geohegan, A. Kane, A. A. Puretzky, C. M. Rouleau, K. L. More, G. T. R. Palmore and R. H. Hurt, Antioxidant deactivation on graphenic nanocarbon surfaces, *Small*, 2011, **7**, 2775–2785.

73 A. F. de Faria, F. Perreault, E. Shaulsky, L. H. Arias Chavez and M. Elimelech, Antimicrobial Electrospun Biopolymer Nanofiber Mats Functionalized with Graphene Oxide-Silver Nanocomposites, *ACS Appl. Mater. Interfaces*, 2015, **7**, 12751–12759.

74 S. S. Nanda, S. S. A. An and D. K. Yi, Oxidative stress and antibacterial properties of a graphene oxide-cystamine nanohybrid, *Int. J. Nanomedicine*, 2015, **10**, 549–556.

75 P. F. M. Nogueira, D. Nakabayashi and V. Zucolotto, The effects of graphene oxide on green algae Raphidocelis subcapitata, *Aquat. Toxicol.*, 2015, **166**, 29–35.

76 H. Xin, Y. Tang, S. Liu, X. Yang, S. Xia, D. Yin and S. Yu, Impact of Graphene Oxide on Algal Organic Matter of Microcystis aeruginosa, *ACS Omega*, 2018, 16969–16975.

77 K. Krishnamoorthy, M. Veerapandian, L. H. Zhang, K. Yun and S. J. Kim, Antibacterial efficiency of graphene nanosheets against pathogenic bacteria via lipid peroxidation, *J. Phys. Chem. C*, 2012, **116**, 17280–17287.

78 L. Kong and R. G. Zepp, Production and consumption of reactive oxygen species by fullerenes, *Environ. Toxicol. Chem.*, 2012, **31**, 136–143.

79 C. Y. Chen and C. T. Jafvert, The role of surface functionalization in the solar light-inducedproduction of reactive oxygen species by single-walled carbon nanotubes in water, *Carbon N. Y.*, 2011, **49**, 5099–5106.

80 T. Dutta, R. Sarkar, B. Pakhira, S. Ghosh, R. Sarkar, A. Barui and S. Sarkar, ROS generation by reduced graphene oxide (rGO) induced by visible light showing antibacterial activity: Comparison with graphene oxide (GO), *RSC Adv.*, 2015, **5**, 80192–80195.

81 D. J. Dwyer, M. A. Kohanski and J. J. Collins, Role of reactive oxygen species in antibiotic action and resistance, *Curr. Opin. Microbiol.*, 2009, **12**, 482–489.

82 L. Barhoumi, A. Oukarroum, L. Ben Taher, L. S. Smiri, H. Abdelmelek and D. Dewez, Effects of Superparamagnetic Iron Oxide Nanoparticles on Photosynthesis and Growth of the Aquatic Plant Lemna gibba, *Arch. Environ. Contam. Toxicol.*, 2015, **68**, 510–520.

83 D. L. Berglund and S. Eversman, Flow cytometric measurement of pollutant stresses on algal cells, *Cytometry*, 1988, **9**, 150–155.

84 N. Miyazawa, M. Hakamada and M. Mabuchi, Antimicrobial mechanisms due to hyperpolarisation induced by nanoporous Au, *Sci. Rep.*, 2018, **8**, 1–8.

85   F. Schwab, T. D. Bucheli, L. P. Lukhele, A. Magrez, B. Nowack, L. Sigg and K. Knauer, Are carbon nanotube effects on green algae caused by shading and agglomeration?, *Environ. Sci. Technol.*, 2011, **45**, 6136–6144.

86   L. Giannuzzi, B. Krock, M. C. C. Minaglia, L. Rosso, C. Houghton, D. Sedan, G. Malanga, M. Espinosa, D. Andrinolo and M. Hernando, Growth, toxin production, active oxygen species and catalase activity of Microcystis aeruginosa (Cyanophyceae) exposed to temperature stress, *Comp. Biochem. Physiol. Part - C Toxicol. Pharmacol.*, 2016, **189**, 22–30.

87   A. Latifi, M. Ruiz and C. Zhang, Oxidative stress in cyanobacteria, 2009, **33**, 258–278.

88   C. M. Rico, J. Hong, M. I. Morales, L. Zhao, A. C. Barrios, J. Y. Zhang, J. R. Peralta-Videa and J. L. Gardea-Torresdey, Effect of cerium oxide nanoparticles on rice: A study involving the antioxidant defense system and in vivo fluorescence imaging, *Environ. Sci. Technol.*, 2013, **47**, 5635–5642.

89   J. Zhao, X. Cao, Z. Wang, Y. Dai and B. Xing, Mechanistic understanding toward the toxicity of graphene-family materials to freshwater algae, *Water Res.*, 2017, **111**, 18–27.

90   O. Akhavan, E. Ghaderi and A. Esfandiar, Wrapping Bacteria by Graphene Nanosheets for Isolation from Environment , Reactivation by Sonication , and Inactivation by Near-Infrared Irradiation, 2011, 6279–6288.

91   Y. Wu, H. Ge and Z. Zhou, Effects of Fructus ligustri lucidi on the growth, cell integrity, and metabolic activity of the Microcystis aeruginosa, *Environ. Sci. Pollut. Res.*, 2015, **22**, 8471–8479.

92   J. Li, D. Ou, L. Zheng, N. Gan and L. Song, Applicability of the fluorescein diacetate assay for metabolic activity measurement of Microcystis aeruginosa (Chroococcales, Cyanobacteria), *Phycol. Res.*, 2011, **59**, 200–207.

93   E. Hoiczyk and A. Hansel, Cyanobacterial cell walls: News from an unusual prokaryotic envelope, *J. Bacteriol.*, 2000, **182**, 1191–1199.